


Article

Electromagnetic Torque Fluctuating Properties under Dynamic RISC Fault in Turbogenerators

Yuling He ¹ , Minghao Qiu ¹, Xinghua Yuan ¹, Haipeng Wang ^{1,*}, Mengya Jiang ¹, Chris Gerada ² and Shuting Wan ¹

¹ Hebei Key Lab of Electric Machinery Maintenance and Failure Prevention, Department of Mechanical Engineering, North China Electric Power University, Baoding 071003, China; heyuling1@ncepu.edu.cn (Y.H.); 220192224062@ncepu.edu.cn (M.Q.); 52451713@ncepu.edu.cn (X.Y.); 220212224028@ncepu.edu.cn (M.J.); 52450809@ncepu.edu.cn (S.W.)

² Power Electronics, Machines and Control (PEMC) Research Group, University of Nottingham, Nottingham NG7 2RD, UK; chris.gerada@nottingham.ac.uk

* Correspondence: 52452403@ncepu.edu.cn

Abstract: This paper analyzes the electromagnetic torque (EMT) fluctuation characteristics in synchronous generators under rotor interturn short-circuit (DRISC) fault. The novelty of this paper is that the DRISC fault is proposed based on the intermittent interturn short circuit existing in the actual operation and compared with the static rotor interturn short-circuit (SRISC) fault. In the work, by studying the influence of DRISC with different positions and different short-circuit degrees, the fluctuation characteristic of the EMT is analyzed and verified. The results show that when the DRISC5% fails, the location is in slot 3, the amplitude of first harmonic decreases by 7.2%, second harmonic amplitude increases by 33.4%, third harmonic decreases by 4.3%, and fourth harmonic increases by 26.8%. As the degree increased and positioned away from the large tooth of the DRISC, the overall EMT amplitude and reverse pulse increased, first and third harmonics decreased, and second and fourth harmonics increased.

Keywords: synchronous generator; dynamic rotor interturn short circuit (DRISC); electromagnetic torque (EMT); magneto-motive force (MMF); harmonic component



Citation: He, Y.; Qiu, M.; Yuan, X.; Wang, H.; Jiang, M.; Gerada, C.; Wan, S. Electromagnetic Torque Fluctuating Properties under Dynamic RISC Fault in Turbogenerators. *Energies* **2022**, *15*, 3821. <https://doi.org/10.3390/en15103821>

Academic Editor: Djaffar Ould-Abdeslam

Received: 11 April 2022

Accepted: 19 May 2022

Published: 23 May 2022

Publisher's Note: MDPI stays neutral with regard to jurisdictional claims in published maps and institutional affiliations.



Copyright: © 2022 by the authors. Licensee MDPI, Basel, Switzerland. This article is an open access article distributed under the terms and conditions of the Creative Commons Attribution (CC BY) license (<https://creativecommons.org/licenses/by/4.0/>).

1. Introduction

Rotor interturn short circuit (RISC) is a common fault, and can usually be divided into dynamic rotor interturn short circuit (DRISC) and static rotor interturn short circuit (SRISC). This kind of fault is usually due to the small radius, and the external insulation part will be broken and cause a short circuit. On the other hand, in the operation of the generator, the high temperature makes the rotor winding expand, causing deformation and displacement. Meanwhile, the generator vibration will lead to insulation damage. Further, the rotor short-circuit failure occurs [1–3].

At present, the domestic and foreign RISC diagnosis method is mainly based on electrical and mechanical parameters. Electrical parameters include stator voltage, stator current [4–6], and parallel branch circulation characteristics [7–9]. The mechanical parameters include unbalanced magnetic tension, stator core vibration, winding vibration characteristics, electromagnetic torque, etc. [10,11].

In terms of the electrical characteristics, Huang et al.'s study concluded that when RISC appears, it will reduce the excitation current, resulting in reactive power [12]. D'Angelo proposed a simulation model of a generator rotor winding detection system, which is a mathematical model established by using the divine network MLP to study the operating power of generator set when RISC appears [13]. Junqing Li et al. analyzed the mathematical expressions of the magnetic momentum and current under RISC conditions and presented the relationship between different harmonic changes of the stator branch current and the

RISC short-circuit position [14]. In [15,16], the stator current and circulation characteristics of the composite failure of the generator are analyzed, and the stator voltage RMS decreases when the RISC occurs. Hao et al. used the multi-loop theorem to obtain an expression for the current of each loop. Both the experiment and simulation met the theoretical analysis, and therefore a method of online fault monitoring using a multi-loop current was obtained [6]. Mazzeletti et al. calculated the stator current difference, obtained the fault correspondence of the residual current vector, and realized the fault diagnosis of RISC for the permanent magnet generator [17].

According to the mechanical characteristics, Albright, D. R. measured the change rate of the air-gap flux density of the rotor by a fixed search coil, which can obtain the short-circuit position more sensitively [18]. In [15], the expression of the unbalanced magnetic pull is obtained by the analysis of the magnetic flux density. Through simulation and experimental verification, the unbalanced magnetic tension makes the generator rotor vibrate at the base frequency under the RISC condition. When RISC occurs, the influence of electromagnetic torque on motor vibration is more obvious. By analyzing the electromagnetic torque under the composite fault of rotor short circuit and eccentric, it was concluded that the generator rotor vibrates at three times the frequency, and the vibration intensifies with the deepening of the fault [16]. Hao used the virtual displacement method to analyze the steady-state harmonic characteristics after EMT failure, and concluded that RISC produces AC pulsation components, which are closely related to the stator winding structure [3]. Hang, J detected the positions of the interturn fault based on the amplitude and initial phase angle of the zero-order voltage component (ZSVC), and proposed a method to directly diagnose the interturn fault by directly collecting the electromagnetic torque [19].

The above literature establishes the basis for the diagnosis of RISC, but rarely studies DRISC. As an improvement, this paper presents a comprehensive study on the EMT fluctuating properties via the new DRISC model with different degrees and positions in synchronous generators. On the basis of comparative studies, variable differences between SRISC and DRISC are further obtained.

2. Analysis Model of DRISC

When the rotor short circuit occurs, the effective turns of the rotor winding decrease, which will affect the decrease of the air-gap magnetic potential. The excitation current in the rotor winding no longer circulates through the fault site and creates a new loop. There will be a reverse current in this loop to create a reverse magnetic potential.

The DRISC from rotor insulation damage over time is investigated by analyzing fault schematics and simplified models, see Figure 1.

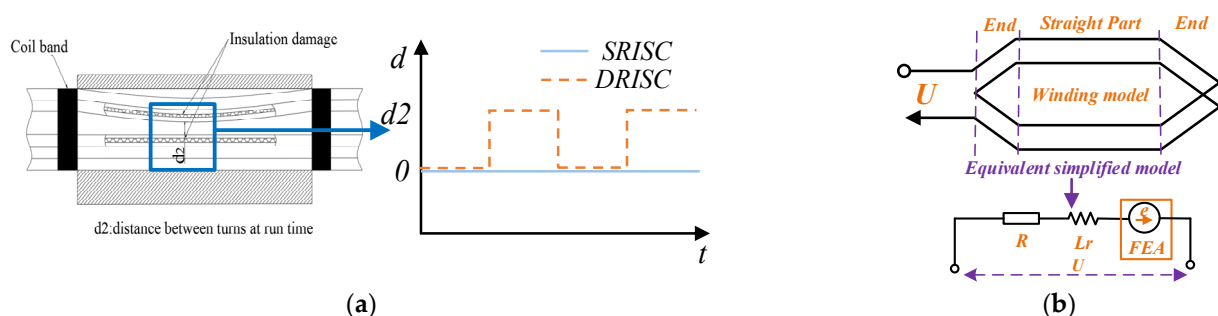


Figure 1. (a) Fault schematic diagram, (b) simplified model.

At the initial stage of short-circuit failure in the generator, intermittent contact occurs at the coil insulation damage. Therefore, in a steady-state excitation circuit, a new circuit occurs in the form of a pulse signal. Moreover, in the late stage of short-circuit fault, the insulation is seriously damaged, and the exposed line is completely touching. Meanwhile, a reverse loop occurs in the excitation circuit, and the reverse signal appears in the form of a step, such as:

$$\begin{aligned} \text{step} & \begin{cases} 0 & \dots \dots t < 0 \\ R_0 & \dots \dots t \geq 0 \end{cases} \\ \text{pulse} & \begin{cases} 0 & \dots \dots t < 0, t > \epsilon \\ \frac{H}{\epsilon} & \dots \dots 0 \leq t \leq \epsilon \end{cases} \end{aligned} \tag{1}$$

The response of the pulse and step signals to a stable system is shown in Figure 2.

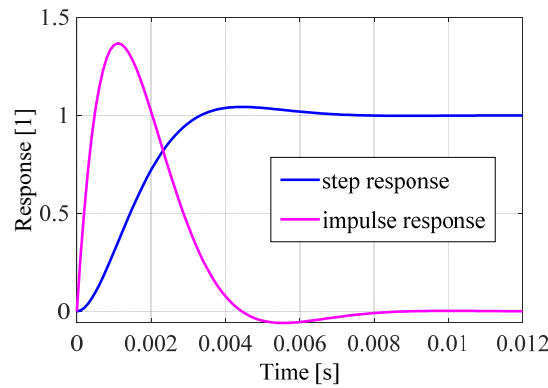


Figure 2. Signal response map.

It is known that the rotor dynamic short circuit is a transient short-circuit process, which can be equivalent to the reverse pulse current generated by the short circuit, resulting in the addition of a reverse pulse magnetic potential based on the original magnetic potential. The static short circuit can be understood as a reverse magnetic potential in generating a step, as shown in Figure 3.

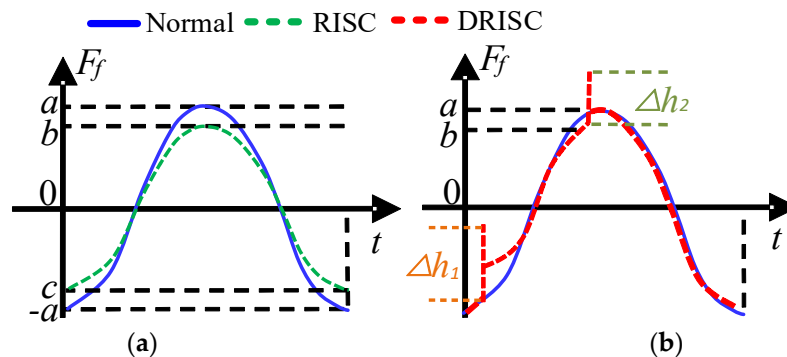


Figure 3. (a) Rotor MMF in SRISC case, (b) rotor MMF in DRISC case.

In DRISC, T is the fault cycle, k is the duty cycle of the short circuit, and h is the peak generated by the short circuit. When the short circuit starts and ends, the h pulse is infinite.

According to the Gaussian magnetic flux theorem, the reverse magnetic potential generated by the reverse current is:

$$F_d(\theta_r) = \begin{cases} -\frac{I_f n_m (2\pi - \alpha_r)}{2\pi} & \dots \dots \beta' \leq \theta_r \leq \beta' + \alpha_r \\ \frac{I_f n_m \alpha_r}{2\pi} & \dots \dots \theta_r < \beta', \theta_r > \beta' + \alpha_r \end{cases} \tag{2}$$

In (2), F_d is the reverse MMF, I_f is the excitation current, n_m is the number of short-circuit turns, θ_r is the circumferential angle of the rotor surface, β' is the starting angle of the groove, where the interturn short circuit occurs, and α_r is the angle of the two grooves, and the angle where the short circuit turns are located.

For a better understanding, the schematic DRISC and the rotor magnetic potential vector diagram are displayed in Figure 4.

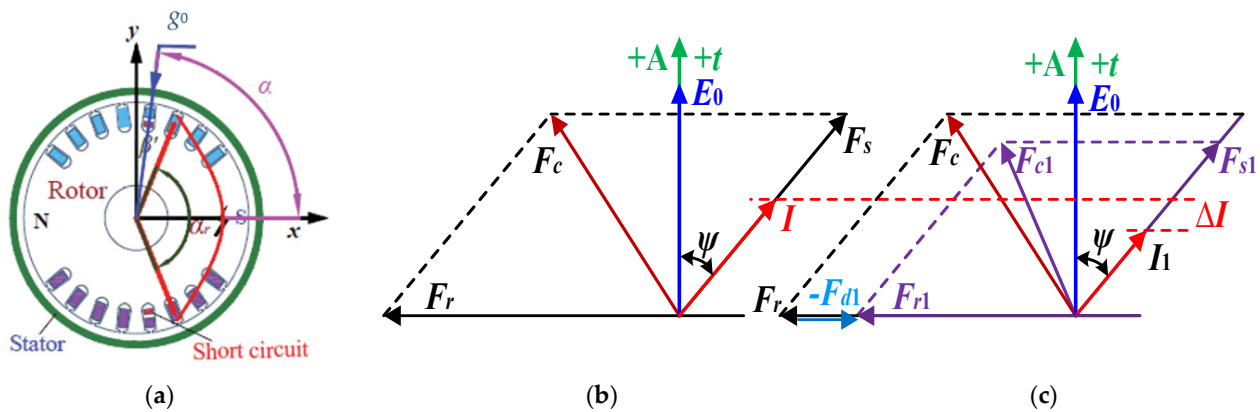


Figure 4. (a) Schematic diagram of short-circuit principle, (b) normal MMF vector, (c) MMF vector under short-circuit conditions.

In Figure 4, F_r is the normal base principal magnetic potential, F_s is the normal armature reaction magnetic potential, and F_c is the synthetic magnetic potential for the composite magnetic potential of the gap base wave. E_o is the empty load potential, I is the positive phase current, and ψ is the internal power angle of the generator. In Figure 4c, the sub-angle marked 1 indicates the parameters after the interturn rotor.

2.1. Impact of DRISC on MFF

The reverse magnetic potential may be expanded by a Fourier series as:

$$\begin{cases} F_d(\theta_r) = A_0 + \sum_{n=1}^{\infty} [A_n \cos(n\theta_r) + B_n \sin(n\theta_r)] \\ A_0 = \frac{1}{2\pi} \int_0^{2\pi} F_d(\theta_r) d\theta_r = 0 \\ A_n = \frac{1}{\pi} \int_0^{2\pi} F_d(\theta_r) \cos(n\theta_r) d\theta_r = -\frac{I_f n_m [\sin(n(\alpha_r + \beta')) - \sin(n\beta')]}{n\pi} \\ B_n = \frac{1}{\pi} \int_0^{2\pi} F_d(\theta_r) \sin(n\theta_r) d\theta_r = \frac{I_f n_m [\cos(n(\alpha_r + \beta')) + \cos(n\beta')]}{n\pi} \end{cases} \quad (3)$$

Moreover, F_d can be represented as:

$$\begin{cases} F_d(\theta_r) = \sum_{n=1}^{\infty} F_{dn} \cos(n\theta_r - \phi) = \sum_{n=1}^{\infty} F_{dn} \cos(n\omega t - \phi_n) \\ F_{dn} = \sqrt{A_n^2 + B_n^2} = \frac{\sqrt{2} I_f n_m}{n\pi} \sqrt{1 - \cos(n\alpha_r)} = \frac{2 I_f n_m}{n\pi} \sin \frac{n\alpha_r}{2} \\ \phi_n = \arctan \frac{B_n}{A_n} = \frac{\cos[n(\alpha_r + \beta)] - \cos(n\beta)}{\sin(n\beta) - \sin[n(\alpha_r + \beta)]} \end{cases} \quad (4)$$

In order to simplify the calculation model, the higher harmonics can be ignored, and only the cases when $n = 1$ (indicating odd harmonic) and $n = 2$ (representing even harmonic) are considered. After the DRISC, the air-gap magnetic potential of the generator is as shown in Figure 4c. F_{d1} and F_{d2} are the base amplitude and second harmonic amplitude of the reverse magnetic potential after the DRISC. Therefore, the magnetic potential after the DRISC can be expressed as:

$$f(\alpha_m, t) = \begin{cases} F_s \cos(\omega t - \alpha_m - \psi - \frac{\pi}{2}) + F_r \cos(\omega t - \alpha_m) \\ = F_c \cos(\omega t - \alpha_m - \gamma_1) \dots \dots \dots \text{Normal} \\ F_{s1} \cos(\omega t - \alpha_m - \psi - \frac{\pi}{2}) + (F_r - F_{d1}) \cos(\omega t - \alpha_m) \\ - F_{d2} \cos 2(\omega t - \alpha_m - \phi_2) \\ = F_{c1} \cos(\omega t - \alpha_m - \gamma_2) - F_{d2} \cos 2(\omega t - \alpha_m - \phi_2) \dots \text{SRISC} \\ \left\{ \begin{array}{l} F_c \cos(\omega t - p\alpha_m) \dots \dots \dots (i-1)T < t < (i-1+k)T \\ \Delta h_1 \dots \dots \dots t = (i-1+k)T \\ F_{c1} \cos(\omega t - p\alpha_m) - F_{d2} \cos 2(\omega t - p\alpha_m) \dots \dots \text{DRISC} \\ \dots \dots \dots (i-1+k)T < t < iT \\ \Delta h_2 \dots \dots \dots t = iT \end{array} \right. \end{cases} \quad (5)$$

It can be seen that when DRISC occurs in the generator, the even harmonic component increases. In the DRISC cycle, during the short circuit and normal state switch, the RMS of the magnetic potential should be between normal and SRISC (SRISC can be considered a special case of DRISC with a duty cycle of 1). Due to the DRISC period of the normal state, the fluctuation of the magnetic potential amplitude will change accordingly.

2.2. Impact of DRISC on MFD

When DRISC occurs, the magnetic tension per unit area remains unchanged, and the magnetic flux density is:

$$B(\alpha_m, t) = \begin{cases} F_c \cos(\omega t - p\alpha_m)\Lambda_0 \cdots \cdots \cdots \text{Normal} \\ [F_{c1} \cos(\omega t - p\alpha_m) - F_{d2} \cos 2(\omega t - p\alpha_m)]\Lambda_0 \cdots \cdots \text{SRISC} \\ \begin{cases} F_c \cos(n\omega t - p\alpha_m)\Lambda_0 \cdots \cdots (i-1)T < t < (i-1+k)T \\ \Delta h_1 \Lambda_0 \cdots \cdots t = (i-1+k)T \end{cases} \\ \begin{cases} [F_{c1} \cos(\omega t - p\alpha_m) - F_{d2} \cos 2(\omega t - p\alpha_m)]\Lambda_0 \cdots (i-1+k)T < t < iT \\ \Delta h_2 \Lambda_0 \cdots \cdots t = iT \end{cases} \\ \cdots \cdots \cdots \text{DRISC} \end{cases} \tag{6}$$

Combined with the previous analysis, the *B* amplitude of the DRISC of the rotor can be seen from (6). In addition to the original odd harmonic component, the harmonic component also increases. With the increase of the short circuit, the amplitude of the original odd subharmonic decreases, and the amplitude of the newly generated even subharmonic increases. There is a pulse at the short-circuit and normal state transition moments, and the overall magnetic density amplitude of DRISC is between normal and SRISC.

As mentioned above, both location and degree will affect the change of the air-gap magnetic density, so the influence on the air-gap magnetic density can be obtained by Formula (7):

$$\begin{cases} F_{d1} = \frac{2I_f}{\pi} n_m \sin \frac{\alpha_r}{2} = \frac{2I_f N}{\pi} \frac{n_m}{N} \sin \frac{\alpha_r}{2} = 0.637 F_r P_s \sin \frac{\alpha_r}{2} \\ F_{d2} = \frac{I_f}{\pi} n_m \sin \alpha_r = \frac{I_f N}{\pi} \frac{n_m}{N} \sin \alpha_r = 0.3185 F_r P_s \sin \alpha_r \\ P_s = \frac{n_m}{N} \end{cases} \tag{7}$$

where *P_s* is the percentage of short circuit (the ratio of short circuit turns, *n_m*, to the total turns, *N*), which can be obtained from Formula (7). As the degree of RISC increases, both *F_{d1}* and *F_{d2}* will increase. When the short circuit is away from the large tooth, *F_{d1}* increases, and *F_{d2}* increases first and then decreases.

2.3. Impact of DRISC on EMT

According to the virtual displacement principle, the EMT studied here can be expressed as:

$$\begin{cases} T = p \frac{\partial W}{\partial \psi} \\ W = \int_v \frac{[B(\alpha_m, t)]^2}{2\mu_0} dv \end{cases} \tag{8}$$

The EMT depends on the square of the MFD. Qualitatively, the trend of EMT should be consistent with MFD, and the trend of the squared operation will be more obvious. Consequently: (1) The appearance of DRISC will reduce the RMS value of EMT, and with the increase of the degree of DRISC, the RMS value of EMT is smaller. (2) The DRISC position also affects the electromagnetic torque, while the farther the DRISC is from the large tooth, the smaller the EMT will be. (3) The appearance of DRISC will bring additional odd harmonics in the electromagnetic torque, because even harmonics are newly produced in MFD, and normally only even harmonics (usually only odd harmonics in MFD, because the DC excitation current can only produce odd harmonics, and the square of MFD only contains even harmonics). The DC component and even harmonics decrease, while the odd harmonics increase. (4) The time domain curve of EMT will be affected by the influence of

the dynamic short-circuit pulse. (5) Under the same position and degree, the SRISC fault has more of an effect on the RMS of EMT than DRISC.

3. FEA and Experimental Validation

In this paper, the CS-5 hidden pole synchronous generator is studied. The finite element calculation and the experimental verification were conducted on the dynamic and static rotor. Parameters are listed in Table 1.

Table 1. Parameters of the CS-5 prototype generator.

Parameters	Values	Parameters	Values
rated power	5 kW	stator core length	130 mm
pole-pairs	1	stator coil turns per slot	22
Power factor ($\cos\varphi$)	0.8	rotor slots	16
radial air-gap length	1.2 mm	rotor core outer diameter	142.6 mm
stator slots	36	rotor core inner diameter	40 mm
stator outer diameter	250.5 mm	rotor coil turns per slot	60
stator inner diameter	145 mm	Internal power factor ($\cos\psi$)	0.62

On the generator, there is a plate with different short-circuit taps. By connecting different taps, varied short-circuit degrees and positions can be simulated, respectively. The tap settings are indicated in Figure 5a. During the experiment, four group tests were performed: (1) common condition without RISC, (2) 5% RISC in slot 1 (L1–L2), (3) 10% RISC in slot 1 (L1–L3), and (4) 10% RISC in slot 2 (L2–L4). Tests (1)–(3) formed a comparison for different short-circuit positions, while (3) and (4) were employed for varied short-circuit degrees.

This prototype generator was specifically designed and manufactured by us, and is able to simulate RISC. This paper establishes the FEA model in ANSYS Maxwell according to the CS-5 hidden pole synchronous generator design parameters, and verifies the stability and convergence of the model through previous calculations.

For vividly simulated failures in the experiment, we treated the photoelectric coupler in the DC solid-state relay as a short-circuit coil. When the photoelectric coupler moves, the short-circuit fault starts. Otherwise, the short-circuit fault ends. For a schematic diagram of the DC solid-state relay, see Figure 5d. During the experiment, the start of the DC solid-state relay was controlled by the PWM. Moreover, the corresponding short-circuit taps were connected by the DC solid-state relay to realize DRISC. In this study, square-wave pulses with a 20 ms period and a forward voltage duty cycle of 15% were generated using PWM. When the square-wave voltage exceeds the DC solid-state relay trigger threshold, the above method can realize the high-frequency DRISC simulation of the generator.

To match of finite element analysis and the experimental settings, the physical model in finite elements was coupled to an external circuit. The external coupling circuit of the generator excitation winding and the armature winding is shown in Figure 5e. S_A1 is a short-circuit trigger switch, setting the trigger voltage interval [V_{on} , V_{off}] to control the short-circuit switch with the pulse voltage source. The dynamic and static rotor interturn short-circuit model can be realized. The pulse time setting of the DRISC is shown in Figure 5c.

To reasonably simulate the short-circuit behavior, the section of the short-circuit winding bar was divided into two components in the 3D model. One is to represent the short-circuit part, and the other is to represent the normal part (see Figure 5b). The short-circuit degree was set by changing the short-circuit turn-numbers of the slot as well as the values of R_f and R_w (see Figure 5e). During simulation, the band rotation was 3000 rpm, the start time was 0 s, the termination time was 0.2 s, and the step size was 0.0002 s.

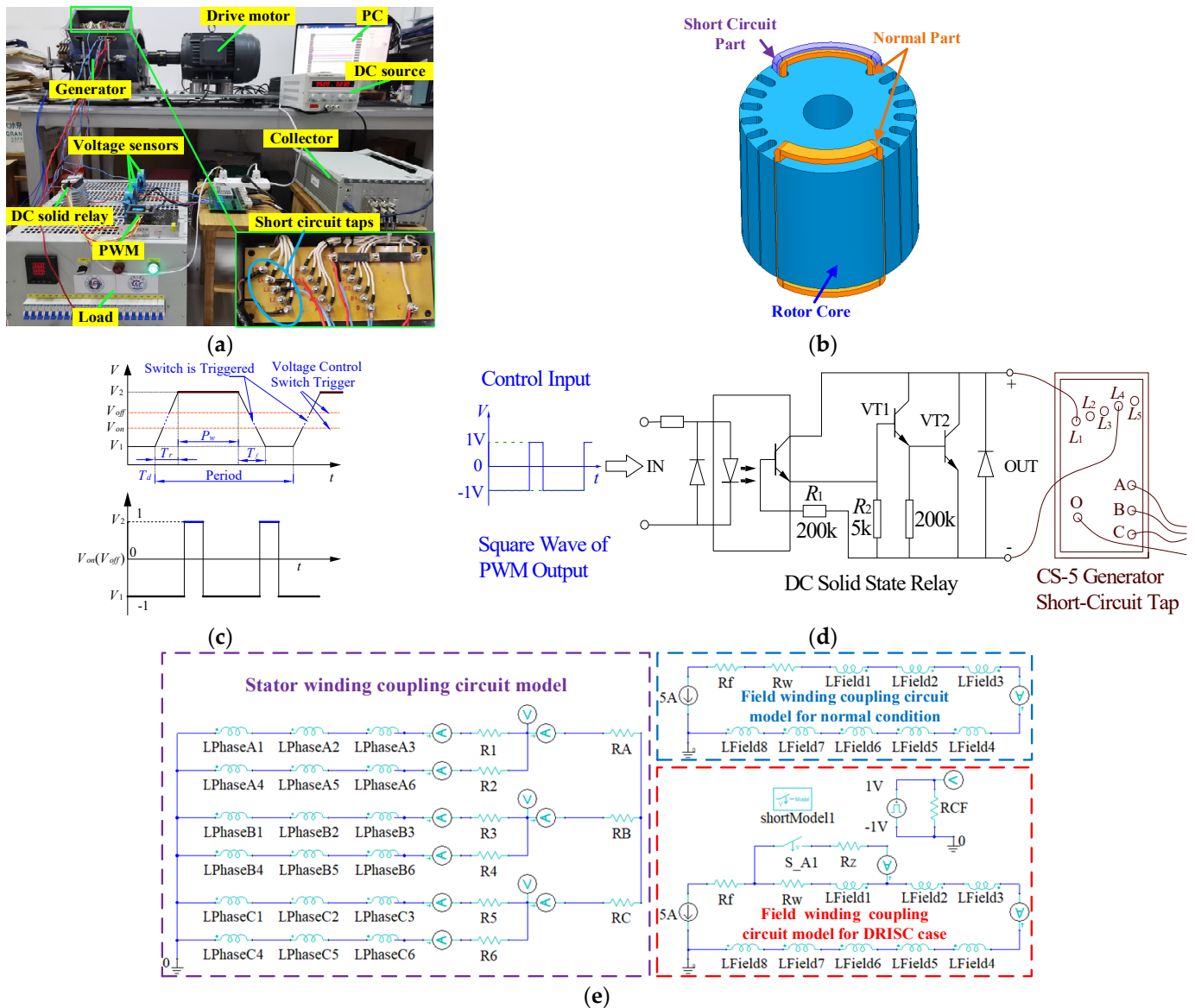


Figure 5. CS-5 generator: (a) picture, (b) FEA model, (c) short-circuit switch control, (d) DRISC trigger circuit, (e) external coupling circuit model.

During the finite element analysis, the external circuit contains parameters such as normal and short-circuit winding and changes the resistance values of the corresponding resistors R_w and R_f . Different degrees of fault simulation can be achieved. In Figure 5c, T_d is the delay time, T_r is the rise time, T_f is the fall time, P_w is the pulse width, the DRISC cycle corresponds to the pulse cycle, and V_{on} is the control switch of the voltage trigger voltage. When the voltage value of the pulse voltage source is greater than V_{on} , the switch S_{A1} acts and the excitation circuit is a short circuit. V_{off} represents the blocking voltage of the voltage control switch. When the voltage value of the pulse voltage source is less than V_{off} , the switch S_{A1} is turned off and the excitation circuit is normal. Both the duty cycle of the short-circuit portion and the DRISC frequency can be changed by adjusting the P_w and the period. The short-circuit portion produced an external circuit of the DRISC with a period of 20 ms (15% duty cycle) under the same settings used in the experiment.

In the experiment, DRISC simulation with different degrees and at different positions can be realized by short-connecting short-circuit taps to different degrees. In the finite element simulation, it corresponds to the experiment by changing the finite element model and the external coupled circuit parameters.

The fault types described in this paper are shown in Table 2. This paper analyzed the harmonic growth ratio on the basis of the normal harmonic amplitude value.

Table 2. Abbreviation of different cases.

Full Name	Abbreviation	Full Name	Abbreviation
Normal	N	DRISC 5%0	D5-0
SRISC 5%3	S5-3	DRISC 5%5	D5-5
SRISC 10%3	S10-3	Short Circuit 5%0	5%0
DRISC 5%3	D5-3	Short Circuit 5%3	5%3
DRISC 10%3	D10-3	Short Circuit 5%5	5%5
SRISC 5%0	S5-0	Short Circuit 10%3	10%3
SRISC 5%5	S5-5		

1. Effect of Short-Circuit Degree

The MFD results at different RISC degrees by finite element analysis are shown in Figure 6. As shown in Figure 6a, the appearance and increase of DRISC decreased the MFD amplitude compared to normal, and the odd harmonic decreased and the even harmonic increased. Compared with SRISC, the appearance of DRISC caused the amplitude fluctuation of the reverse pulse produced by the short circuit. As the degree of the short circuit intensified, the pulse impact became greater. The equivalent degree of DRISC failure had less effect on harmonics than SRISC, but with the same trend (see Figure 6b). This result is consistent with a previous theoretical analysis (see Equation (15)). The EMT results of the FEM model and experiments established in this paper are shown in Figure 7. It is shown that odd harmonic and amplitude pulses occurred when DRISC occurred. As shown by the FEA curve in Figure 7d,e, when the short circuit 5% occurred, the amplitude of first harmonic decreased by 7.2%, second harmonic amplitude increased by 33.4%, third harmonic decreased by 4.3%, and fourth harmonic increased by 26.8%. With the increase of DRISC degree, the total electromagnetic torque amplitude, constant component amplitude, and second harmonic amplitude decreased, while the fourth harmonic and pulse amplitude increased. The reason for the amplitude fluctuation spikes in EMT is that DRISC generated reverse pulses in the original stable excitation circuit. The reverse pulse increased as the short circuit increased.

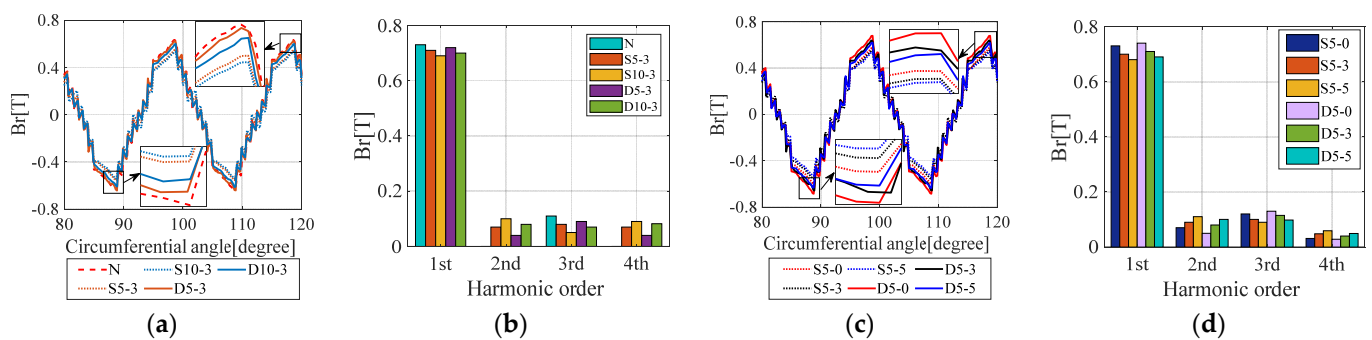


Figure 6. MFD variations: (a,b) varied dynamic short-circuit degrees, (c,d) varied dynamic short-circuit positions.

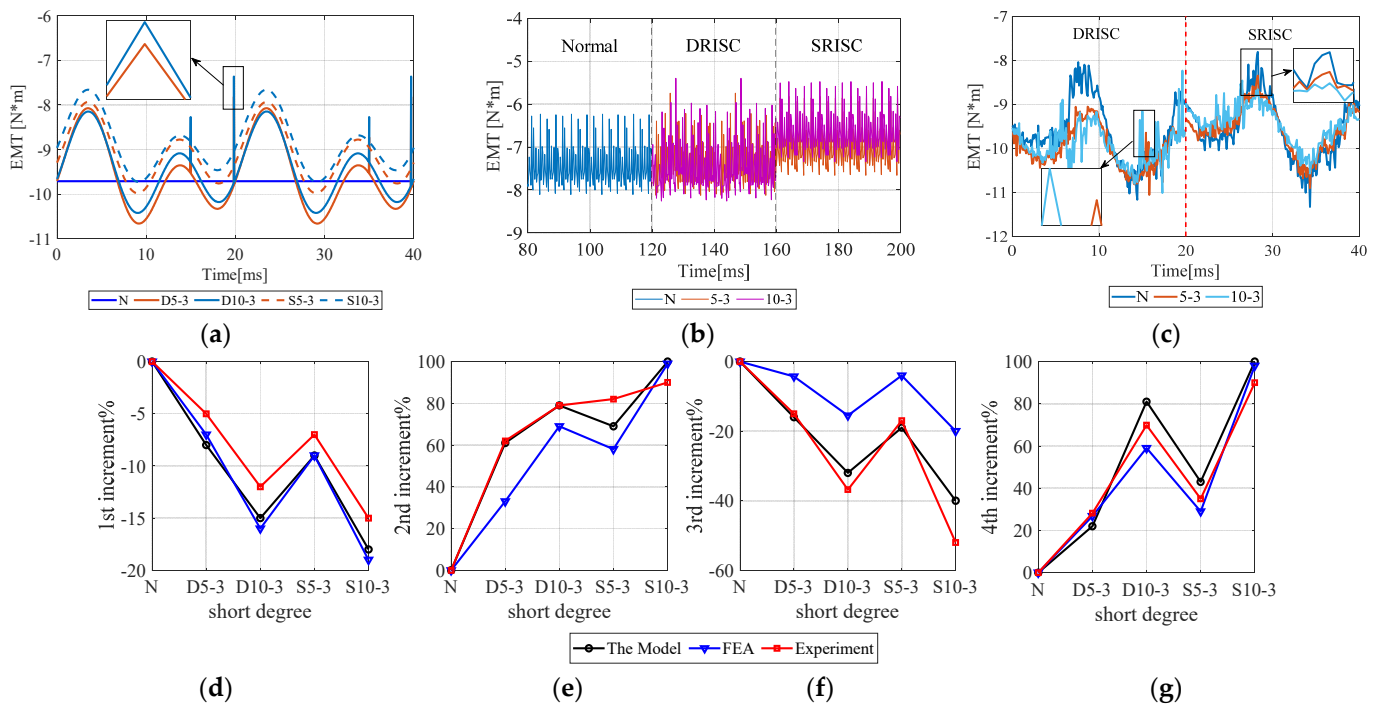


Figure 7. EMT in varied DRISC degree cases: (a–c) waves by model, FEA, and experiment, and (d–g) harmonic variations.

Compared to SRISC, the amplitude of the EMT second harmonics decreased by 17.6% and fourth harmonic decreased by 10.8% when the same degree of DRISC failure occurred. The theoretical analysis, FEA, and experiment had the same trends.

2. Effect of Short-Circuit Position

The results of the finite element model analysis are shown in Figure 6. When DRISC occurred and the position was far from the large tooth, the reverse magnetic potential generated by the short circuit had a greater influence on the rotor excitation potential. The overall amplitude of the MFD was compressed, with the odd harmonic component increasing and the even harmonic component decreasing. When the DRISC occurred, the MFD curve had a smaller amplitude pulse compared with the SRISC.

The EMT obtained from the proposed model and from the finite element analysis and experiments are shown in Figure 8. It can be seen that the odd harmonic component appeared when the DRISC fault occurred. When the DRISC5% fault position changed from slot 3 to slot 5, the amplitude of first harmonic decreased by 42.5%, second harmonic amplitude increased by 11.4%, third harmonic decreased by 19.4%, and fourth harmonic increased by 32.3%. With the short-circuit position away from the large tooth, the total electromagnetic torque amplitude, constant component amplitude, and second harmonic component amplitude will decrease, while the fourth harmonic and reverse amplitude pulse value will increase. This is consistent with the qualitative analysis conclusion obtained by (19).

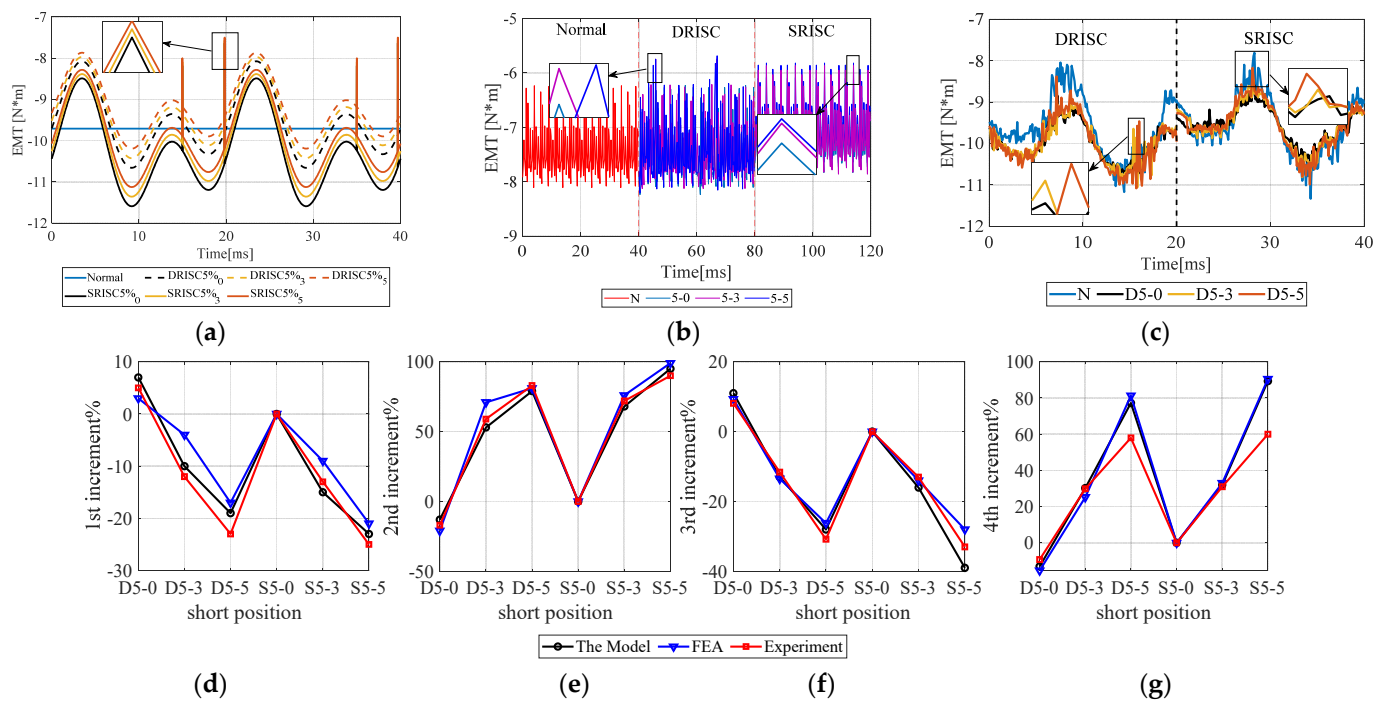


Figure 8. EMT in varied DRISC position cases: (a–c) waves by model, FEA, and experiment, and (d–g) harmonic variations.

4. Conclusions

This paper presented a new analytical model for RISC fault in synchronous generators. Further, the EMT fluctuations were comprehensively studied based on the proposed DRISC model with different degrees and positions. Using the CS-5 fault simulation generator for the analysis, the FEA calculation and the experimental tests confirmed the validity and the eligibility of the proposed model. The results showed that:

- (1) When the DRISC5% failed, the location was in slot 3, the amplitude of first harmonic decreased by 7.2%, second harmonic amplitude increased by 33.4%, third harmonic decreased by 4.3%, and fourth harmonic increased by 26.8%. As the degree of the DRISC increased, the overall EMT amplitude and reverse pulse increased, first and third harmonics decreased, and second and fourth harmonics increased.
- (2) When the DRISC5% fault position changed from slot 3 to slot 5, the amplitude of first harmonic decreased by 42.5%, second harmonic amplitude increased by 11.4%, third harmonic decreased by 19.4%, and fourth harmonic increased by 32.3%. At the DRISC position away from the large tooth, the overall EMT amplitude and reverse pulse increased, first and third harmonics decreased, and second and fourth harmonics increased.
- (3) Compared with SRISC, DRISC had less influence on the EMT amplitude and each harmonic, but the electromagnetic torque curve showed obvious amplitude pulse.
- (4) When a DRISC failure occurred, significant amplitude spikes appeared in the EMT curve. As the DRISC failure intensified and the fault was away from the large tooth, the reverse pulse generated by the short circuit became larger. Therefore, the vibration amplitude of the EMT became larger.

Author Contributions: Writing—original draft, M.Q.; Writing—review & editing, Y.H., X.Y., H.W., M.J., C.G. and S.W. All authors have read and agreed to the published version of the manuscript.

Funding: This research was funded by [National Natural Science Foundation of China] grant number [51777074] and [National Natural Science Foundation of China] grant number [52177042].

Conflicts of Interest: The authors declare no conflict of interest.

References

1. Dirani, H.C.; Merkhouf, A.; Kedjar, B.; Giroux, A.M.; Al-Haddad, K. Rotor interturn short circuit impact on large hydrogenerator magnetic quantities. *IEEE Trans. Ind. Appl.* **2018**, *54*, 3702–3711. [\[CrossRef\]](#)
2. Valavi, M.; Jørstad, K.G.; Nysveen, A. Electromagnetic analysis and electrical signature-based detection of rotor inter-turn faults in salient-pole synchronous machine. *IEEE Trans. Magn.* **2018**, *54*, 1–9. [\[CrossRef\]](#)
3. Hao, L.; Wu, J.; Zhou, Y. Theoretical analysis and calculation model of the electromagnetic torque of nonsalient-pole synchronous machines with interturn short circuit in field windings. *IEEE Trans. Energy Convers.* **2014**, *30*, 110–121. [\[CrossRef\]](#)
4. Hang, J.; Ding, S.; Zhang, J.; Cheng, M.; Chen, W.; Wang, Q. Detection of Interturn Short-Circuit Fault for PMSM With Simple Fault Indicator. *IEEE Trans. Energy Convers.* **2016**, *31*, 1697–1699. [\[CrossRef\]](#)
5. Park, Y.; Jeong, M.; Lee, S.B.; Antonino-Daviu, J.A.; Teska, M. Influence of Blade Pass Frequency Vibrations on MCSA-Based Rotor Fault Detection of Induction Motors. *IEEE Trans. Ind. Appl.* **2017**, *53*, 2049–2058. [\[CrossRef\]](#)
6. Hao, L.; Sun, Y.; Qiu, A.; Wang, X. Steady-State Calculation and Online Monitoring of Interturn Short Circuit of Field Windings in Synchronous Machines. *IEEE Trans. Energy Convers.* **2011**, *27*, 128–138. [\[CrossRef\]](#)
7. Li, G.-J.; Hloui, S.; Ojeda, J.; Hoang, E.; Lecrivain, M.; Gabsi, M.; Zhu, Z.Q. Excitation Winding Short-Circuits in Hybrid Excitation Permanent Magnet Motor. *IEEE Trans. Energy Convers.* **2014**, *29*, 567–575. [\[CrossRef\]](#)
8. Dorrell, D.G.; Makhoba, K. Detection of Inter-Turn Stator Faults in Induction Motors Using Short Term Averaging of Forwards and Backwards Rotating Stator Current Phasors for Fast Prognostics. *IEEE Trans. Magn.* **2017**, *53*, 1–7. [\[CrossRef\]](#)
9. Yucai, W.; Yonggang, L.; Heming, L.; Wenjing, Z. An Analysis of the Impact of Rotor Winding Interturn Short Circuits on Turbine Generator Operating Variables. *Electr. Power Compon. Syst.* **2015**, *43*, 674–684. [\[CrossRef\]](#)
10. Chai, F.; Li, Y.; Pei, Y.; Yu, Y. Analysis of Radial Vibration Caused by Magnetic Force and Torque Pulsation in Interior Permanent Magnet Synchronous Motors Considering Air-Gap Deformations. *IEEE Trans. Ind. Electron.* **2018**, *66*, 6703–6714. [\[CrossRef\]](#)
11. He, Y.-L.; Deng, W.-Q.; Tang, G.-J. Analysis and Simulation on UMP and EMT Characters of Turbogenerator under Axial Air-Gap Eccentricity. *Int. J. Rotating Mach.* **2015**, *2015*, 1–10. [\[CrossRef\]](#)
12. Huang, H.; Zhang, K.; Zhang, Y. Detection of turbine generator field winding serious inter-tum short circuit based on the rotor vibration feature. In Proceedings of the International Universities Power Engineering, Glasgow, UK, 1–4 September 2009; pp. 1–5.
13. D’Angelo, M.F.; Costa, P.P. Detection of shorted turns in the field winding of turbogenerators using the neural network MLP. In Proceedings of the IEEE International Conference on Systems, Tucson, AZ, USA, 7–10 October 2001; pp. 1930–1935.
14. Li, J.; Shi, W.; Li, Q. Research on interturn short circuit fault location of rotor winding in synchronous electric machines. In Proceedings of the International Conference on Electrical Machines and Systems, Sydney, NSW, Australia, 11–14 August 2017; pp. 1–4. [\[CrossRef\]](#)
15. He, Y.L.; Wang, F.L.; Ke, M.Q.; Tang, G.J. Rotor vibration difference among the single and the combined faults composed by static air-gap eccentricity and rotor interturn short circuit. In *Proceedings of the 9th IFToMM International Conference on Rotor Dynamics*; Springer: Cham, Switzerland, 2015.
16. Shuting, W.; Yonggang, L.; Heming, L.; Guiji, T.A. Compositive Diagnosis Method on Turbine-Generator Rotor Winding Inter-turn Short Circuit Fault. In Proceedings of the 2006 IEEE International Symposium on Industrial, Electronics, Montreal, QC, Canada, 9–13 July 2006; pp. 1662–1666.
17. Mazzoletti, A.; Bossio, G.R.; De Angelo, C.H.; Espinoza-Trejo, D.R. A Model-Based Strategy for Interturn Short-Circuit Fault Diagnosis in PMSM. *IEEE Trans. Ind. Electron.* **2017**, *64*, 7218–7228. [\[CrossRef\]](#)
18. Albright, D.R. Interturn short-circuit detector for turbine generator rotor windings. *IEEE Trans. Power Appar. Syst.* **1971**, *90*, 478–483. [\[CrossRef\]](#)
19. Hang, J.; Ding, S.; Ren, X.; Hu, Q.; Huang, Y.; Hua, W.; Wang, Q. Integration of interturn fault diagnosis and torque ripple minimization control for direct-torque-controlled SPMSM drive system. *IEEE Trans. Power Electron.* **2021**, *36*, 11124–11134. [\[CrossRef\]](#)